Facile synthesis and characterisation of uniform and monodispersed $In(OH)_3$ and In_2O_3 microcubes

Zhenhe Xu[1] ✉, Junying Lin[1], He Yu[1], Yaguang Sun[1], Fu Ding[2], Hongtao Fan[1], Shan Shi[3], Qinghong Fang[3], Yanfeng Bi[4], Yu Gao[3]

[1]*The Key Laboratory of Inorganic Molecule-Based Chemistry of Liaoning Province, College of Applied Chemistry, Shenyang University of Chemical Technology, Shenyang, 110142, People's Republic of China*
[2]*College of Chemical Engineering, Shenyang University of Chemical Technology, Shenyang, 110142, People's Republic of China*
[3]*College of Materials Science and Engineering, Shenyang University of Chemical Technology, Shenyang, 110142, People's Republic of China*
[4]*College of Chemistry, Chemical Engineering and Environmental Engineering, Liaoning Shihua University, Fushun 113001, People's Republic of China*
✉ *E-mail: xuzh@syuct.edu.cn*

Published in Micro & Nano Letters; Received on 21st February 2017; Revised on 1st May 2017; Accepted on 9th May 2017

$In(OH)_3$ microcubes have been successfully synthesised by a direct precipitation in solution at room temperature without using any surfactant or template. Furthermore, the In_2O_3 microcubes were obtained through calcining the $In(OH)_3$ microcubes. The results show that the as-prepared $In(OH)_3$ and In_2O_3 products have a cube shape with a mean edge length of 190 and 155 nm, respectively. The self-assembly process via orientation attachment is proposed in order to explain the growth mechanism for the microcubes. Upon ultraviolet excitation, a broad blue photoluminescence emission with its maximum intensity centred at 466 nm is shown, which is due to the oxygen deficiencies in the In_2O_3 microcubes. It endows these microcubes with potential application, such as liquid crystal devices, solar-energy conversion, optical and electric devices.

1. Introduction: Nowadays, inorganic micro/nanomaterials with well-defined morphologies and accurately tunable sizes have stimulated great interest because the morphology, dimensionality, and size of materials are closely correlated with the physicalcochemical properties of materials [1–3]. Thus, extensive efforts have been devoted to develop new methods for the synthesis of a range of high-quality inorganic micro/nanomaterials, such as hydrothermal method, sol–gel processes, chemical vapour technique, and so forth [4, 5]. Among them, precipitation route has been proved to be a convenient and an effective method for synthesis of various inorganic micro/nanomaterials with well-defined morphology [6–8]. During the precipitation process, materials are not only synthesised in large quantities with a desired morphology, composition, size, but also are prepared by using green, environmentally responsible methodologies.

In recent years, indium oxide (In_2O_3) which is a very important wideband-gap (direct band gap around 3.6 eV), n-type transparent semiconductor has been extensively studied due to its potential applications such as solar cells, liquid-crystal display [9], photocatalyst [10, 11], and ultrasensitive gas sensor for detection of O_3 [12], CO_2 [13], NO_2 [14], HCHO [15], acetone [16], and Cl_2 [15]. To date, various morphologies of In_2O_3 have been fabricated via different methods. For example, In_2O_3 nanoparticles synthesised by nanosecond laser ablation in water [17], In_2O_3 nanobelts prepared by thermal evaporation [18], In_2O_3 nanowries manufactured by using a laser ablation approach [19], In_2O_3 whiskers prepared by physical vapour deposition process [20], In_2O_3 nanowire and nanorods synthesised by template-assisted growth [21, 22]. Despite these endeavours, it is challenging to explore more facile, efficient, and low-cost methods to fabricate large-scale and well-crystallised In_2O_3 micro/nanomaterials to both scientific research and industrial applications.

In the present work, we reported a simple method for the synthesis of $In(OH)_3$ microcubes from the mixture of aqueous solution of $InCl_3$ and KOH at room temperature. A possible formation mechanism of the microcubes was proposed. Through calcinating the $In(OH)_3$ microcubes, the In_2O_3 microcubes with the same morphology have been obtained. Finally, the optical property of the resulting In_2O_3 microcubes was investigated.

2. Experimental

2.1. Materials: All chemicals were analytical grade reagents and used as purchased without further purification. The water used in the experiments was ultra-purified water (18.25 MΩ). $InCl_3{\cdot}4H_2O$ and KOH were purchased from Sinopharm Chemical Reagent Co., Ltd.

2.2. Preparation of In_2O_3 microcubes: In a typical synthesis, 2 mmol of $InCl_3{\cdot}4H_2O$ and 5.0 g KOH were dissolved in 10 mL of H_2O, respectively. Then, the KOH aqueous solution was added into the $InCl_3$ solution, and it was stirred for 2 h in an open system. The resulting suspension was placed at room temperature for 5 days without further stirring or shaking. The product was then separated by centrifugation, washed with ethanol and distilled water for several times, and dried in atmosphere at 60°C for 4 h. The conversion of as-prepared $In(OH)_3$ to In_2O_3 was carried out in an over at 900°C for 4 h in air.

2.3. Characterisation: The X-ray diffraction (XRD) patterns of the samples were recorded on a D8 focus diffractometer (Bruker) with Cu Kα radiation ($\lambda = 0.15405$ nm). Thermogravimetric data were recorded with thermal analysis instrument (SDT 2960, TA Instruments, New Castle, DE) with the heating rate of 10°C min^{-1} in an air flow of 100 mL min^{-1}. The morphologies of the as-prepared samples were inspected using a field emission scanning electron microscope (FESEM, S4800, Hitachi) equipped with energy-dispersive X-ray (EDX) spectrometer. The photoluminescence (PL) spectra were recorded with a Hitachi F-7000 spectrophotometer equipped with a 150 W xenon lamp as the excitation source. All the measurements were performed at room temperature.

3. Results and discussion: Fig. 1*A* shows the XRD pattern of the as-prepared $In(OH)_3$ sample which can be indexed to a cubic lattice [space group: $Im\bar{3}(204)$] of pure indium hydroxide. The calculated lattice constant, $a = 0.7977$ nm, is in good agreement with the standard JCPDS (Card No. 85-1338, $a = 0.7979$ nm). Figs. 1*B* and *C* show the SEM images of the as-formed $In(OH)_3$ microcubes. It can be seen that the $In(OH)_3$ sample is composed of uniform and monodisperse microcubes. It can be calculated that the mean edge length is about 190 nm. The high-magnification SEM image (Fig. 1*C*) shows the surfaces of sample are very rough, implying that the microcubes consist of many small nanoparticles. The chemical composition of the $In(OH)_3$ microcubes indicates that the microcubes are made of In and O and the molar ratio of In to O is approximately equal to 1: 3 (Fig. 1*D*).

Well-dispersed and uniform $In(OH)_3$ microcubes were used as precursor to fabricate In_2O_3 sample. We firstly investigated the effect of calcination on the crystallisation and morphology of the as-prepared $In(OH)_3$ sample. On the basis of TGA data (Fig. 2), $In(OH)_3$ sample was calcined from room temperature to 900°C with a total weight loss of 27.99% and maintained at this temperature for 4 h for ensuring their complete decomposition. The XRD pattern (Fig. 3*A*) of the resulting sample exhibits that all of peaks can be perfectly indexed to the cubic phase [space group: $Ia\bar{3}(206)$] of In_2O_3. The calculated lattice parameter ($a = 1.0120$ nm) for In_2O_3, is similar to the known lattice parameter for standard In_2O_3 ($a = 1.0117$ nm; JCPDS Card No. 71-2194). Furthermore, the

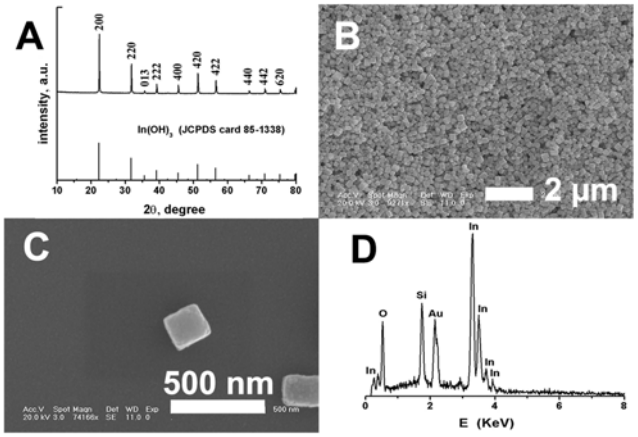

Fig. 1 *XRD pattern, SEM image, and EDX of the In(OH)₃ sample*
A XRD pattern of the as-formed $In(OH)_3$ sample. The standard data for $In(OH)_3$ (JCPDS Card No. 85-1338) is also presented in the figures for comparison
B and C SEM images of the as-formed $In(OH)_3$ sample
D EDX of the as-formed $In(OH)_3$ sample

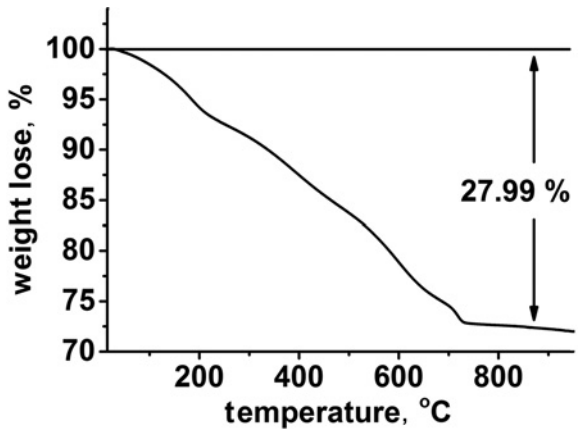

Fig. 2 *TGA curve of the as-formed In(OH)₃ sample*

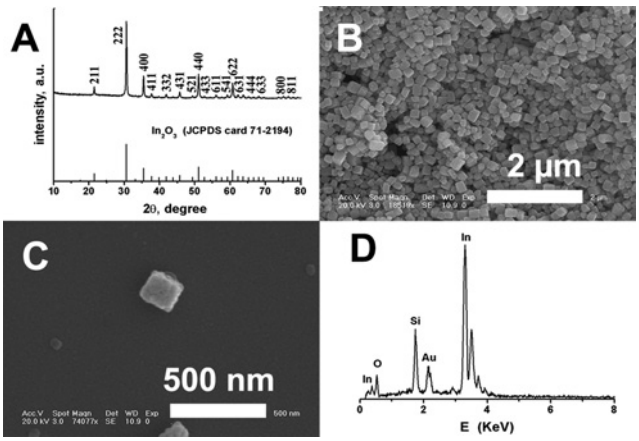

Fig. 3 *XRD pattern, SEM image, and EDX of the In₂O₃ sample*
A XRD pattern of the as-formed In_2O_3 sample. The standard data for In_2O_3 (JCPDS Card No. 71-2194) is also presented in the figures for comparison
B and C SEM images of the as-formed In_2O_3 sample
D EDX of the as-formed In_2O_3 sample

crystallite size of the $In(OH)_3$ and In_2O_3 products can be estimated from the Scherrer equation, $D = 0.941\lambda/\beta \cos\theta$, where D is the average grain size, λ is the X-ray wavelength (0.15405 nm), and θ and β are the diffraction angle and full-width at half-maximum of an observed peak, respectively [23]. The estimated average crystallite sizes are about 60 nm for $In(OH)_3$ particles and 50 nm for In_2O_3 particles, which were calculated by the strongest peaks (200) at $2\theta = 22.33°$ and (222) at $2\theta = 30.64°$, respectively. In addition, no peaks of impurities have been found in the XRD patterns of the $In(OH)_3$ and In_2O_3 products, which indicates the high purity of the products. Meanwhile, the strong and sharp peaks indicate that the as-obtained products are highly crystallised. After calcination at 900°C, the SEM image shows that the obtained In_2O_3 sample retain the morphology of the $In(OH)_3$ precursor (Fig. 3*B*), and the product consists of large-scale, monodisperse microcubes with a mean edge length of 155 nm. Compared to $In(OH)_3$ microcubes, the size of the In_2O_3 sample is slightly shrunk since the density of the In_2O_3 sample is increased. Furthermore, careful observation reveals (Fig. 3*C*) that the obtained In_2O_3 microcubes show that there are many cracks on the surfaces of the In_2O_3 microcubes, which may be attributed to the removal of H_2O molecule from the $In(OH)_3$ microcubes during the calcination process. The EDX spectrum (Fig. 3*D*) shows the presence of In and O with an atomic ratio of In to O is approximately equal to 2:3.

In principle, the degree of supersaturation, the diffusion of the reaction, the species to the surface of the crystals, the surface and interfacial energies, and the structure of the crystals govern the growth and morphology of crystal [6]. Hence the effects of different reaction factors on the microcubes have been discussed, such as the amount of KOH and reaction times. Of particular interest is that the molar ratio of $InCl_3$/KOH played a significant role in adjusting the final morphologies in this work. Fig. 4 shows the SEM images of the $In(OH)_3$ samples obtained when we introduced different amounts of KOH (from 0.5 to 5 g) into the reaction. When the amount of KOH was 0.5 g, the resultant morphology was entirely composed of nanoparticles, as shown in Fig. 4*A*. As the amount of KOH increases to 1.5 g, some poorly developed microcubes as well as a great many of tiny nanoparticles could be found (Fig. 4*B*). Upon further increasing the amount of KOH to 3.0 g, the product consisted of nearly monodispersed microcubes and some irregular agglomeration (Fig. 4*C*). When 5.0 g of KOH was added to the reaction solution, the morphology of the product was composed of monodisperse microcubes, and the quality was greatly improved (Fig. 4*D*). Based on the above results, we can come to the conclusion that with the amount of KOH gradually

doi: 10.1049/mnl.2017.0090

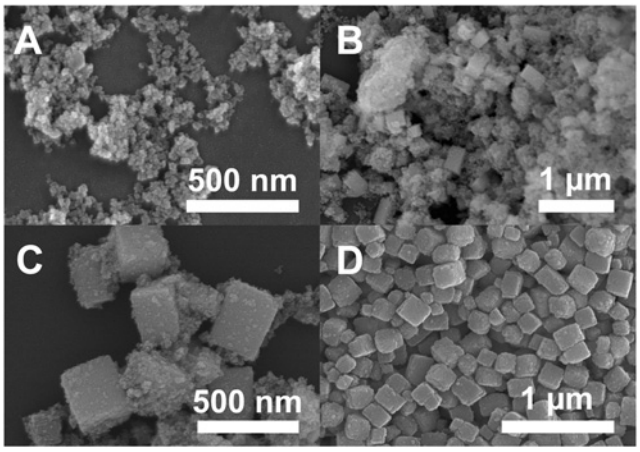

Fig. 4 *SEM images of the $In(OH)_3$ samples obtained at different amount of KOH*
A 0.5 g
B 1.5 g
C 3.0 g
D 5.0 g

increasing, the morphologies of the microcubes become uniform, monodispersity, and the optimal amount of KOH for the formation of $In(OH)_3$ is 5 g.

Time-dependent morphological evolution experiments of $In(OH)_3$ were carried out, and the corresponding intermediate samples were characterised by SEM technique to study their growth behaviour. Fig. 5 provides the SEM images of the $In(OH)_3$ microcubes prepared at different reaction time with otherwise the same synthetic conditions. As shown in Fig. 5*A*, the morphology of the sample is fully composed of irregular nanoparticles when the reaction time is 5 h. Furthermore, some nanoparticles aggregate together to form larger clusters, and other morphologies cannot be detected. When the reaction is prolonged to 24 h, the morphology of the corresponding sample is composed of a few poor developed microcubes as well as many larger aggregations (Fig. 5*B*). With the time increasing to 72 h, more microcubes appear at the expense of the nanoparticles, and they are poorly developed with rough surface (Fig. 5*C*). Upon further increasing the time to 120 h, due to the continuous growth, the poorly developed $In(OH)_3$ microcubes gradually grow into regular microcubes with a well-defined shape (Fig. 5*D*).

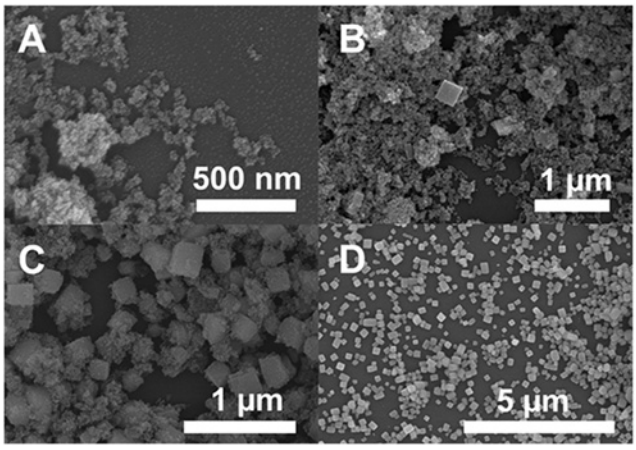

Fig. 5 *SEM images of the $In(OH)_3$ samples obtained at different reaction time*
A 5 h
B 24 h
C 72 h
D 120 h

According to the time-dependent experiment results, the formation of $In(OH)_3$ microcubes belongs to aggregation growing process. The aggregation growing process reveals that the formation of uniform micro/nanomaterials usually precede in several stages [24]. In the initial stage, a supersaturated solution leads to the nucleation. Then, the growth of the nuclei via a diffusive mechanism forms crystalline subunits, which, in turn, aggregate to form the larger assemblages. Hence, $In(OH)_3$ nanoparticles are obtained through the direct reaction between $InCl_3$ and KOH aqueous solution. Then, the $In(OH)_3$ nanoparticles are rearranged to find a suitable place for minimising the surface energy of nanoparticles. Those crystal nuclei aggregates in different direction (random aggregation), rotated, and twisted simultaneously to form $In(OH)_3$ microcubes. The whole process of formation microcubes is illustrated in Fig. 6. Finally, $In(OH)_3$ microcubes can be converted to In_2O_3 microcubes via the subsequent calcination, while morphology doesn't change during the conversion. It must be pointed out that such a transformation is common for $In(OH)_3$ compound decomposition [23, 25].

The photoluminescence properties of the as-prepared $In(OH)_3$ and In_2O_3 samples were also investigated. First, the $In(OH)_3$ microcubes don't show any photoluminescence under ultraviolet (UV) light excitation. But, the In_2O_3 microcubes exhibit a broad photoluminescence with its maximum intensity centred at 466 nm under UV light irradiation (Fig. 7). It is well-known that bulk In_2O_3 crystals cannot emit any photoluminescence at room temperature [25]. Yet, the In_2O_3 nanostructures can emit UV and visible light, such as In_2O_3 nanoparticles with photoluminescence spectra peaking at 480 and 520 nm [26]. It is generally accepted that the oxygen vacancies in oxide semiconductors result the PL emission. Thus, in our study, the In_2O_3 microcubes emit the blue photoluminescence because of the radiative recombination of an electron occupying oxygen vacancies with a photoexcited hole.

4. Conclusion: In summary, we have developed a facile synthetic route to synthesise $In(OH)_3$ and In_2O_3 microcubes. The shape and size of $In(OH)_3$ samples can be modulated by the amount of

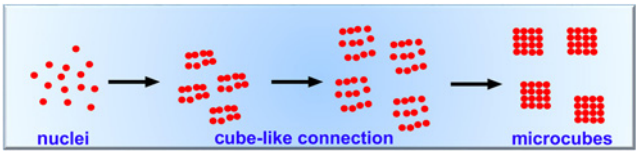

Fig. 6 *Illustration for the formation process of the $In(OH)_3$ microcubes*

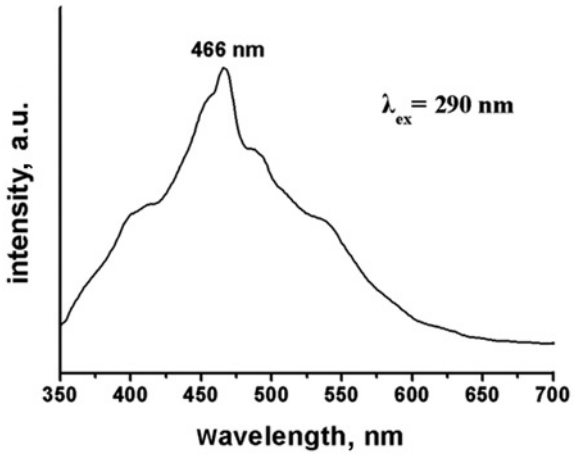

Fig. 7 *Photoluminescence emission spectrum of the In_2O_3 microcubes under an excitation wavelength of 290 nm*

KOH and reaction time, respectively. The formation mechanism for the $In(OH)_3$ microcubes bases on a self-assembly process of nanoparticles via oriented attachment. The as-formed $In(OH)_3$ microcubes do not show any photoluminescence, while the as-synthesised In_2O_3 microcubes exhibit a strong blue emission because of the oxygen vacancies. It endows these microcubes with potential application, such as solar cells, liquid crystal devices, optical, and electric devices. Furthermore, this facile and environmentally friendly method may be further expanded to the large-scale synthesis of other oxide or non-oxide architectures for the advanced applications.

5. Acknowledgments: This work was supported by the National Natural Science Foundation of China (grant nos. NSFC 51402198, 21477082, 21671139, and 21301170), the Natural Science Foundation of Liaoning Province (grant nos. 201602592 and 20170540715), Educational Bureau of Liaoning Province for the Fundamental Research of Key Lab (grant nos. LZ2014028, LZ2016003), Liaoning Natural Science Foundation Combined with Open Foundation of Shenyang National Laboratory for Materials Sciences (grant no. s2015021019).

6 References

[1] Xu Z., Quintanilla M., Vetrone F., *ET AL.*: 'Harvesting lost photons: plasmon and upconversion enhanced broadband photocatalytic activity in Core@Shell microspheres based on lanthanide-doped $NaYF_4$, TiO_2, and Au', *Adv. Funct. Mater.*, 2015, **25**, pp. 2950–2960

[2] Xu Z., Liu Y., Ren F., *ET AL.*: 'Development of functional nanostructures and their applications in catalysis and solar cells', *Coord. Chem. Rev.*, 2016, **320–321**, pp. 153–180

[3] Kim M.R., Xu Z., Chen G., *ET AL.*: 'Semiconductor and metallic core-shell nanostructures: synthesis and applications in solar cells and catalysis', *Chem. Eur. J.*, 2014, **20**, pp. 11256–11275

[4] Chen G., Rosei F., Ma D.: 'Template engaged synthesis of hollow ceria-based composites', *Nanoscale*, 2015, **7**, pp. 5578–5591

[5] Zhang L., You H., Yang M., *ET AL.*: 'Core/Shell $Y(OH)CO_3:Eu^{3+}$/$YBO_3:Eu^{3+}$ phosphors with sphericity, submicrometre size and non-aggregation characteristics', *Micro Nano Lett.*, 2011, **6**, pp. 728–731

[6] Xu Z., Li C., Yang P., *ET AL.*: 'Uniform $Ln(OH)_3$ and Ln_2O_3 (Ln = Eu, Sm) submicrospindles: facile synthesis and characterization', *Cryst. Growth Des.*, 2009, **9**, pp. 4127–4135

[7] Zhang J., Xu J., Zhang H., *ET AL.*: 'Chemical synthesis of $SrCO_3$ microcrystals via a homogeneous precipitation method', *Micro Nano Lett.*, 2011, **6**, pp. 205–208

[8] Xing L., Peng L.: 'Comparison of preparation and formation mechanism of luag nanopowders using two different methods', *Micro Nano Lett.*, 2012, **7**, pp. 529–532

[9] Hamberg I., Granqvist C.G.: 'Evaporated Sn-doped In_2O_3 films: basic optical properties and applications to energy-efficient windows', *J. Appl. Phys.*, 1986, **60**, pp. R123–R160

[10] He L., Wood T.E., Wu B., *ET AL.*: 'Spatial separation of charge carriers in $In_2O_{3-x}(OH)_y$ Nanocrystal superstructures for enhanced gas-phase photocatalytic activity', *ACS Nano*, 2016, **10**, (5), pp. 5578–5586

[11] Wu M., Wang C., Zhao Y., *ET AL.*: 'Hydrothermal synthesis of porous rh-In_2O_3 nanostructures with visible-light-driven photocatalytic degradation of tetracycline', *CrystEngComm*, 2015, **17**, pp. 2336–2345

[12] Gagaoudakis E., Bender M., Douloufakis E., *ET AL.*: 'The influence of deposition parameters on room temperature ozone sensing properties of inox films', *Sens. Actuator B-Chem.*, 2001, **80**, pp. 155–161

[13] Chung W.Y., Sakai G., Shimanoe K., *ET AL.*: 'Preparation of indium oxide thin film by spin-coating method and its gas-sensing properties', *Sens. Actuator B-Chem.*, 1998, **46**, pp. 139–145

[14] Liess M.: 'Electric-field-induced migration of chemisorbed gas molecules on a sensitive film-a new chemical sensor', *Thin Solid Films*, 2002, **410**, pp. 183–187

[15] Tamaki J., Naruo C., Yamamoto Y., *ET AL.*: 'Sensing properties to dilute chlorine gas of indium oxide based thin film sensors prepared by electron beam evaporation', *Sens. Actuator B-Chem.*, 2002, **83**, pp. 190–194

[16] Lian H., Wang G., Yue H., *ET AL.*: 'Enhanced acetone sensing properties of Eu-In_2O_3 nanotubes with bumps', *Micro Nano Lett.*, 2016, **11**, pp. 825–827

[17] Ismail R.A.: 'Preparation of colloidal In_2O_3 nanoparticles using nanosecond laser ablation in water', *Micro Nano Lett.*, 2011, **6**, pp. 951–954

[18] Pan Z.W., Dai Z.R., Wang Z.L.: 'Nanobelts of semiconducting oxides', *Science*, 2001, **291**, pp. 1947–1949

[19] Li C., Zhang D., Han S., *ET AL.*: 'Diameter-controlled growth of single-crystalline In_2O_3 nanowires and their electronic properties', *Adv. Mater.*, 2003, **15**, pp. 143–146

[20] Yumoto H., Sako T., Gotoh Y., *ET AL.*: 'Growth mechanism of vapor-liquid-solid (VLS) grown indium tin oxide (ITO) whiskers along the substrate', *J. Cryst. Growth.*, 1999, **203**, pp. 136–140

[21] Zheng M.J., Zhang L.D., Li G.H., *ET AL.*: 'Ordered indium-oxide nanowire arrays and their photoluminescence properties', *Appl. Phys. Lett.*, 2001, **79**, pp. 839–841

[22] Kuo C.Y., Lu S.Y., Wei T.Y.: 'In_2O_3 Nanorod formation induced by substrate structure', *J. Cryst. Growth.*, 2005, **285**, pp. 400–407

[23] Yang J., Lin C., Wang Z., *ET AL.*: '$In(OH)_3$ and In_2O_3 nanorod bundles and spheres: microemulsion-mediated hydrothermal synthesis and luminescence properties', *Inorg. Chem.*, 2006, **45**, pp. 8973–8979

[24] Wang S., Song S., Deng R., *ET AL.*: 'Hydrothermal synthesis and upconversion photoluminescence properties of lanthanide doped YF_3 sub-microflowers', *CrystEngComm*, 2010, **12**, pp. 3537–3541

[25] Tang Q., Zhou W., Zhang W., *ET AL.*: 'Size-controllable growth of single crystal $In(OH)_3$ and In_2O_3 nanocubes', *Cryst. Growth Des.*, 2005, **5**, pp. 147–150

[26] Zhou H., Cai W., Zhang L.: 'Photoluminescence of indium–oxide nanoparticles dispersed within pores of mesoporous silica', *Appl. Phys. Lett.*, 1999, **75**, pp. 495–497

doi: 10.1049/mnl.2017.0090